

Photon-assisted conditionality for double-dot charge qubits in a single-mode cavity

Alexander V. Tsukanov*

Institute of Physics and Technology, Russian Academy of Sciences, Nakhimovsky prospekt 34, Moscow, 117218, Russia

(Received 20 October 2011; published 30 January 2012)

The problems of the design, control, and interaction of the single-electron double-dot charge qubits coherently coupled to the optical cavity mode are studied theoretically. A way to overcome the challenges concerned with the use of classical laser pulses for a qubit state engineering is described, replacing the lasers by a quantized photon field in a semiconductor cavity and a gate voltage. Using this strategy, a simple and efficient scheme is proposed for the creation of highly entangled multiqubit states like the nine-qubit Shor states.

DOI: [10.1103/PhysRevA.85.012331](https://doi.org/10.1103/PhysRevA.85.012331)

PACS number(s): 03.67.Mn, 42.50.Dv, 78.67.Hc

I. INTRODUCTION

Semiconductor quantum dots (QDs), often termed as artificial atoms, are widely studied objects in both theoretical and experimental physics [1]. The possibility to form ordered QD assemblies together with plausible control of spectral and coherent properties of individual QDs make them very promising systems for quantum information purposes [2], especially for single-photon sources [3] and quantum bit (qubit) embodiments (see, e.g., Refs. [4–9]). Usually, the QD-based qubits are divided into three groups (i.e., the charge [4,5], spin [6,7], and exciton [8,9] qubits). Particularly, in the charge qubits quantum information is stored in electron orbital states of the QD confining potential. Any qubit state transformation can be organized by classic optical excitations [4] and/or by electrostatic voltages [5]. On other hand, one may also exploit an empty QD (logical zero) and QD with a single bound electron-hole pair (logical one) as the exciton qubit [8,9]. The transition between its logical states is performed by a short (~ 1 ps) laser pulse [9] with frequency corresponding to the electron-hole pair generation energy (~ 1 eV). This frequency domain is easily accessible with commercial lasers. Besides, the QDs are extensively integrated into solid-state photonic devices such as high-quality quantum electrodynamics cavities and waveguides. This field-matter interface enables one to address optical (electron or exciton) transitions in the single QD with the help of the cavity photons. Up to now, several prototypes of quantum computation devices relying upon single QDs embedded in microresonators (toroids or spheres) and in defects in photonic crystals have been realized experimentally [10–21]. The discovery of such an optical driving force (i.e., a quantized electromagnetic field in the cavity) opens another (distinct from that using the classical field) way of qubit control and allows one to perform single-qubit rotations under near-field regime by variation of the QD frequency relative to the cavity frequency (or vice versa). The field strength generated by a single cavity photon may be as large as 10 V/cm in antinodes, which is enough for fast implementation of quantum operations. Moreover, the cavity can modify the QD electron or exciton lifetime due to the Purcell effect [21].

An alternative strategy for the charge qubit design and control was proposed by Openov [22] and developed in

papers [23–27] by later researchers. In his proposal, the qubit logical states are presented by electron orbital states localized in the conduction band of a symmetric double quantum dot (DQD). Quantum operations are driven by the laser whose frequency is resonant to the transition between logical states and an auxiliary state delocalized over the whole structure. The frequency of the electron transitions lies in the terahertz range ($\sim 50 - 100$ meV). Since the logical states are the ground states of the DQD, this qubit is expected to be much more stable than the single QD charge qubit [4] or the exciton qubit [8]. However, many authors believe such optical mechanisms of charge qubit state control to be quite difficult for realization in practice because of the absence of reliable terahertz coherent sources.

Here, we propose a scheme for quantum control and entanglement of localized charge states of single-electron DQDs placed in a semiconductor cavity. Earlier improvement of optically driven charge qubits by means of cavity exploiting was made by the authors of Ref. [28]. However, their proposal, together with the cavity and the gate voltages, still required the use of a terahertz laser. Our study is aimed at overcoming the challenges inherent to the laser-driven DQD charge qubit by full replacement of the laser with the cavity field and the gate voltage as it was already done theoretically in Ref. [29] for the DQD exciton qubits. In view of recent experimental advances in the design and fabrication of these systems, one is able to achieve the desired terahertz frequency domain by an appropriate choice of the geometry and material of the cavity. Hence, required engineering of the electron DQD state can be carried out by means of the control over its frequency by electrostatic gating without the laser. As we show, a single photon in the cavity mode can be employed as a driver for electronic transitions in the DQD thus providing the single-qubit rotations. Further, making use of conditional absorption of the cavity photon by the first (control) qubit, one can stop the evolution of the second (target) qubit. This effect will be utilized in nontrivial two-qubit operations like the controlled-NOT (CNOT) gate. The strength of such indirect photon-mediated coupling between qubits does not depend on the interqubit distance. Therefore, one gains an ability to weaken the crosstalks by placing the qubits as far as possible from each other. Note that the cavity initialization (viz., its population by the single photon) may be achieved via the electrostatic injection of a single electron from the substrate to the excited QD level and its subsequent relaxation

*tsukanov@ftian.ru

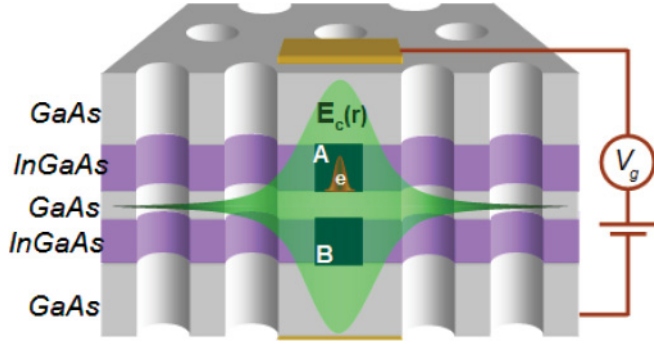


FIG. 1. (Color online) The schematics of the double quantum dot (DQD) placed in the antinode of single-photon cavity field $\mathbf{E}_c(\mathbf{r})$. The cavity is lithographically arranged in InGaAs/GaAs heterostructure-based two-dimension photonic crystal due to several hole omission (line defect). The InAs QDs A and B are formed in InGaAs layers separated by GaAs barrier. The electron is initially localized in the ground state of the QD A . Its orbital state is controlled by the voltage V_g on the gate plates.

to the QD ground state with single-photon emission into the cavity mode. This mechanism resembles that exploited in heterostructure-based cascade lasers and assures flexible control of the emitted photon frequency by electrostatic means as well. Finally, the qubit state measurement may be performed with the help of modern high-sensitivity charge sensors [30] or, alternatively, via diverse photon detection techniques.

The paper is organized as follows. In Sec. II we introduce the model and the formalism describing coherent evolution of the charge qubit in the cavity. Section III contains the description of how to realize several important quantum gates and the numerical simulations. The perspectives of application of the results obtained are discussed in Sec. IV. We conclude our study in Sec. V.

II. THE MODEL

Consider a single-electron DQD composed of a pair of two-level, nearly identical QDs, A and B , and placed in the body of a single-mode cavity, as shown in Fig. 1. In the figure, the cavity is presented by the defect in the two-dimensional photonic crystal; however, the formalism developed in the paper is valid for arbitrary quantum single-mode resonators. The QD ground states, $|A0\rangle$ and $|B0\rangle$, are well isolated from each other while their excited states, $|A1\rangle$ and $|B1\rangle$, are

coupled by electron tunneling. The Hamiltonian that describes the DQD and the cavity has the form

$$\begin{aligned} H &= H_q + H_c, \\ H_q &= \sum_{k=A0,A1,B0,B1} \varepsilon_k |k\rangle \langle k| - V(|A1\rangle \langle B1| + |B1\rangle \langle A1|) \\ &\quad + (g_A |A0\rangle \langle A1| a^\dagger + g_B |B0\rangle \langle B1| a^\dagger + \text{H.c.}), \\ H_c &= \hbar \omega_c a^\dagger a, \end{aligned} \quad (1)$$

where $\varepsilon_k \equiv \varepsilon_k(t)$ are the energies of the DQD single-electron states $|k\rangle$ ($k = A0, A1, B0, B1$), $V \equiv V(t) > 0$ is the tunneling matrix element between the DQD excited states $|A1\rangle$ and $|B1\rangle$, $g_{A(B)} = \langle A(B)0| - e \mathbf{E}_c \mathbf{r} |A(B)1\rangle$ is the coupling coefficient between the cavity field and the single QD optical transition $|A0\rangle \leftrightarrow |A1\rangle$ ($|B0\rangle \leftrightarrow |B1\rangle$), \mathbf{r} is the electron position, $\mathbf{E}_c \equiv \mathbf{E}_c(\mathbf{r})$ is the cavity field strength, e is the electron charge, ω_c is the cavity mode frequency, $a = \sum_{n=0}^{\infty} \sqrt{n} |n-1\rangle \langle n|$ is the photon annihilation operator, n is the photon number in the cavity, and \hbar is the Planck constant (in what follows, $\hbar \equiv 1$). Equation (1) represents the generalized Jaynes-Cummings Hamiltonian, where the counter-rotating terms are dropped since we suppose that $|g_{A(B)}| \ll \omega_c$. Next, the QD relaxation and cavity dissipation rates, γ and Γ_c , are believed small when compared to the couplings $g_{A(B)}$ to attain the strong-coupling regime. Besides, all of the time-dependent parameters in Eq. (1) are supposed to be smooth enough at the photon bouncing time $\tau' \sim \omega_c^{-1}$.

Let the cavity mode be initially populated by a single photon while the DQD is loaded into one of its ground states (or their superposition). The Hamiltonian (1) provides coherent exchange by a single quantum between the DQD and the cavity. Therefore, the DQD-cavity state vector can be expressed as

$$\begin{aligned} |\Psi\rangle &= c_{A0,1} \exp[-i\varphi_{A0}(t) - i\omega_c t] |A0,1\rangle \\ &\quad + c_{B0,1} \exp[-i\varphi_{B0}(t) - i\omega_c t] |B0,1\rangle \\ &\quad + c_{A1,0} \exp[-i\varphi_{A1}(t)] |A1,0\rangle \\ &\quad + c_{B1,0} \exp[-i\varphi_{B1}(t)] |B1,0\rangle. \end{aligned} \quad (2)$$

In this expression, $c_{A0,1}$, $c_{B0,1}$, $c_{A1,0}$, and $c_{B1,0}$ are the time-dependent probability amplitudes of the electron-photon states $|k,n\rangle$ ($n = 0, 1$) and $\varphi_k = \int_0^t \varepsilon_k(t') dt'$ are the corresponding phases. By substitution of Eq. (2) into the Schrödinger equation, $i\partial_t |\Psi\rangle = H |\Psi\rangle$, one obtains following system for the probability amplitudes:

$$i\partial_t \begin{pmatrix} c_{A0,1} \\ c_{B0,1} \\ c_{A1,0} \\ c_{B1,0} \end{pmatrix} = \begin{pmatrix} 0 & 0 & g_A \exp(i\delta\varphi_A) & 0 \\ 0 & 0 & 0 & g_B \exp(i\delta\varphi_B) \\ g_A^* \exp(-i\delta\varphi_A) & 0 & 0 & -V \exp(i\delta\Delta) \\ 0 & g_B^* \exp(-i\delta\varphi_B) & -V \exp(-i\delta\Delta) & 0 \end{pmatrix} \begin{pmatrix} c_{A0,1} \\ c_{B0,1} \\ c_{A1,0} \\ c_{B1,0} \end{pmatrix}. \quad (3)$$

Here, we introduce the phase differences $\delta\varphi_{A(B)} = \int_0^t \delta_{A(B)}(t') dt'$ and $\delta\Delta = \int_0^t \Delta(t') dt'$ through the detuning $\delta_{A(B)}(t) = \omega_c - \omega_{A(B)}(t)$ of the resonant frequency $\omega_{A(B)}(t) = \varepsilon_{A(B)1}(t) - \varepsilon_{A(B)0}(t)$ of the QD A (B) from the cavity mode frequency ω_c and the difference $\Delta(t) = \varepsilon_{A1}(t) - \varepsilon_{B1}(t)$ of excited state energies, respectively. The DQD energy diagrams, Fig. 2, visualize those parameters.

The changes in the QD energies and in the interdot tunneling can be produced by variation of the QD confining potential with the help of the bias voltage applied across the DQD [5,19,20,29]. We assume such voltage-driven pulses to have square form with Gaussian wings characterized by the envelope function

$$f_g(t, \tau_0, \tau_p) = \{1 - \exp(-t^2/\tau_0^2) - \exp[-(t - \tau_p)^2/\tau_0^2]\} \times [\Theta(t) - \Theta(t - \tau_p)], \quad (4)$$

where τ_0 is the pulse elevation and drop time, $\tau_p \gg \tau_0$ is the pulse duration time, and $\Theta(t)$ is the Heaviside

function. Let us choose the frequencies of both QDs be far detuned from the cavity frequency at the beginning and at the end of the pulse: $|\delta_{A(B)m}| = |\omega_c - \omega_{A(B)m}| \gg |g_{A(B)}|$, where $\omega_{A(B)}(0) = \omega_{A(B)}(\tau_p) \equiv \omega_{A(B)m}$. This means that the coupling between the QDs and the cavity is negligible and the DQD evolves freely. Otherwise, if $\tau_0 \leq t \leq \tau_p - \tau_0$, the QD $A(B)$ becomes coupled to the cavity field with some detuning $\delta_{A(B)0}$. In this case, the detuning as a function of time can be given by the formula $\delta_{A(B)}(t) = \delta_{A(B)0} + [\delta_{A(B)m} - \delta_{A(B)0}][1 - f_g(t, \tau_0, \tau_p)]$, and we obtain following expression for the phase difference $\delta\varphi_{A(B)}$:

$$\delta\varphi_{A(B)} = \begin{cases} \delta_{A(B)0}t + \frac{\sqrt{\pi}}{2}[\delta_{A(B)m} - \delta_{A(B)0}]\tau_0[\Phi(\frac{t}{\tau_0}) + \Phi(\frac{\tau_p}{\tau_0}) + \Phi(\frac{t-\tau_p}{\tau_0})], & 0 \leq t \leq \tau_p \\ \delta_{A(B)0}\tau_p + \sqrt{\pi}[\delta_{A(B)m} - \delta_{A(B)0}]\tau_0\Phi(\frac{\tau_p}{\tau_0}) + \delta_{A(B)m}(t - \tau_p), & t > \tau_p, \end{cases} \quad (5)$$

where $\Phi(x) = \frac{2}{\sqrt{\pi}} \int_0^x \exp(-\xi^2) d\xi$ is the error function. In a similar way, the tunneling and the energy difference are given by the formulas $V(t) = V_0 + (V_m - V_0)[1 - f_g(t, \tau_0, \tau_p)]$ and $\Delta(t) = \Delta_0 + (\Delta_m - \Delta_0)[1 - f_g(t, \tau_0, \tau_p)]$, respectively, where $V_{0(m)}$ and $\Delta_{0(m)}$ are the corresponding values when the pulse is switched on (off). The phase accumulated due to the excited state energy difference behaves as

$$\delta\Delta = \begin{cases} \Delta_0t + \frac{\sqrt{\pi}}{2}(\Delta_m - \Delta_0)\tau_0[\Phi(\frac{t}{\tau_0}) + \Phi(\frac{\tau_p}{\tau_0}) + \Phi(\frac{t-\tau_p}{\tau_0})], & 0 \leq t \leq \tau_p \\ \Delta_0\tau_p + \sqrt{\pi}(\Delta_m - \Delta_0)\tau_0\Phi(\frac{\tau_p}{\tau_0}) + \Delta_m(t - \tau_p), & t > \tau_p. \end{cases} \quad (6)$$

In order to simplify our model, we suppose that the electrostatic control does not change the couplings g_A and g_B . The next serious assumption concerns the excited state

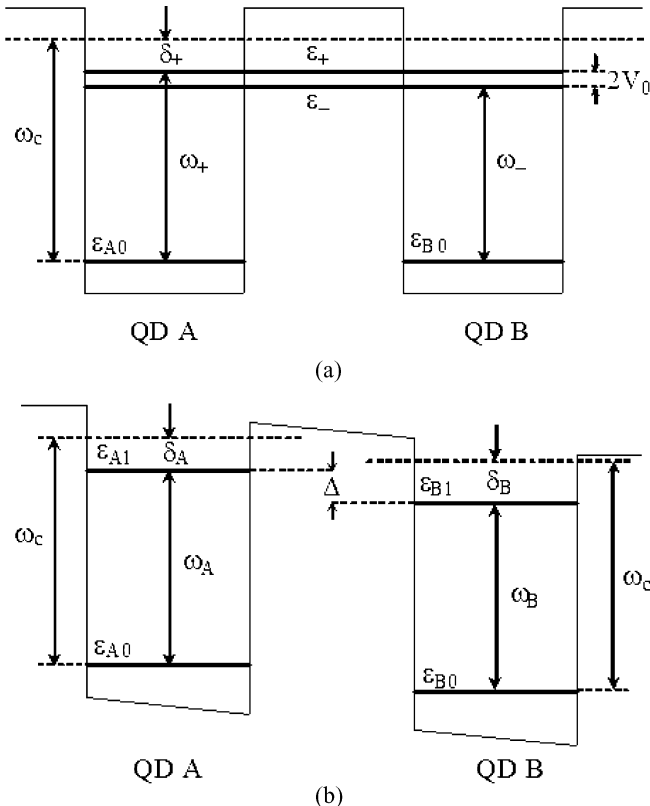


FIG. 2. Energy profiles of DQD for (a) symmetric and (b) asymmetric voltage driving (see text for details).

energy difference, which can be also expressed as $\Delta = \delta_A - \delta_B + \varepsilon_{A0} - \varepsilon_{B0}$. As it follows from the perturbation theory, the energy shift is proportional to the zero-order energy. Therefore, for deep QDs, the voltage-induced shifts of delocalized excited states are expected to be much greater than that of localized ground states. This allows us to set $\varepsilon_{A0} \approx \varepsilon_{B0}$ and to replace Δ by the detuning difference, $\Delta \approx \delta_A - \delta_B$. Of course, in the general DQD model one should take into account the ground-state energy difference as an additional independent parameter.

An analytical solution of Eq. (3) was found in Ref. [27] for the case of identical QDs A and B subjected to the laser-driven ramp pulses ($\tau_0 \rightarrow 0$). Here, we study this equation numerically for the voltage-driven pulses with the envelope given by Eq. (4). Below we show how the pulse and structure parameters have to be chosen to organize the desired quantum evolution of the qubits.

III. QUANTUM OPERATIONS

First, we check the robustness of our DQD being used as a quantum memory cell. This means that the electron state vector should conserve its initial state over quite a long time interval. In analogy to Refs. [22–27], we identify the logical qubit states with the DQD ground states: $|0\rangle \equiv |A0\rangle$ and $|1\rangle \equiv |B0\rangle$. In order to protect the qubit in the absence of the pulse from unwanted evolution (optical transition and/or level shift) caused by the cavity photon one has to choose (i) the frequency detunings to be large compared to the coupling coefficients, $|g_{A(B)}| \ll |\delta_{A(B)m}|$, and (ii) the tunneling to be small compared to the excited state energy difference, $V_m \ll |\Delta_m|$. In this case, the DQD dynamics is reduced to the nonresonant evolution of independent QDs [27] that amounts only to negligible electron excitation from the ground

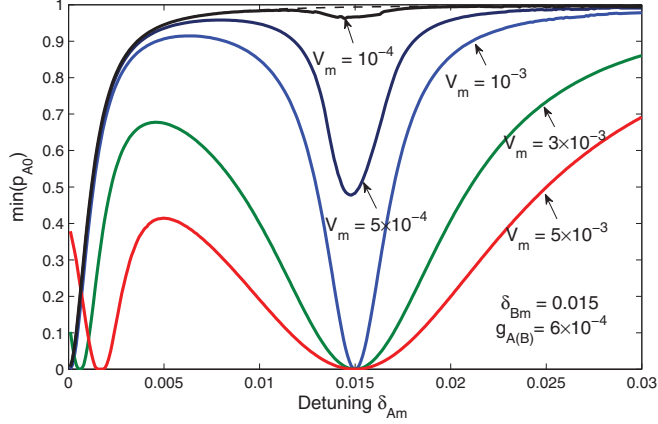


FIG. 3. (Color online) The minimum of the population p_{A0} of the stored DQD state $|A0\rangle$ at different detunings and tunnelings. The value of minimum is calculated over the time interval $0 \leq t \leq \Gamma_c^{-1}$. All parameters in the plot are given in units of ω_c .

states and to small phase accumulation. To illustrate the ability of information storage, we plot the minimum of the population $p_{A0} = |c_{A0}|^2$ of the initial state $|A0\rangle$ ($c_{A0}(0) = 1$) as a function of the detuning δ_{Am} at fixed detuning δ_{Bm} for several values of tunneling V_m . The amplitude error is concerned with population leakage from given state via cavity-stimulated excitation processes. Therefore, it is enough to consider the qubit parasite evolution during the photon lifetime. For this purpose, Eq. (3) was numerically integrated at the time interval $0 \leq t \leq \Gamma_c^{-1} = Q/\omega_c$, where we have used an optimistic value $Q = 10^6$ for the resonator quality. The results of simulations are visualized in Fig. 3 for the equal coupling case, $g_A = g_B \equiv g = 6 \times 10^{-4} \omega_c$.

One sees that for highly symmetric DQD (i.e., for which $\delta_{Am} \approx \delta_{Bm}$) the population p_{A0} is fully squeezed to other states even at large detunings (here, $\delta_{Bm} = 0.015 \omega_c$) due to the off-resonant electron excitation. With that, the tunneling suppression ($V_m < 10^{-4} \omega_c$) brings about the localization of the population in the initial state with probability $p_{A0} > 0.99$ for almost all detunings except for the narrow interval around the symmetry point. For very small tunnelings, the storage reliability is well characterized by the single-QD ground-state population $p_{A0} = \delta_{Am}^2 / (4|g_A|^2 + \delta_{Am}^2)$ (dashed curve in Fig. 3). On other hand, the cavity produces phase shifts

$$\delta\theta_{A(B)} = -|g_{A(B)}|^2 t / \delta_{A(B)m} \quad (7)$$

of the logical states. Those phase errors can be neglected for symmetric DQD where $\delta\theta_A = \delta\theta_B$ and relative phase shift, $\delta\theta = \delta\theta_A - \delta\theta_B$, is zero. However, as we have just seen, the symmetry amounts to the growth of amplitude error at moderate V_m . Thus, we may recommend to keep $\delta\theta_A \approx \delta\theta_B$ at small tunnelings $V_m < 10^{-4} \omega_c$ in order to suppress the quantum errors of both types during the information storage.

Next, we consider the single-qubit rotations around polar and azimuth axes of the Bloch sphere (population inversion and phase shift, respectively). The inversion of population of logical states is equivalent to the NOT operation. Its successful implementation in a single-electron DQD requires meeting several conditions, as was found earlier [22–27]. First, it is necessary to tune the energies of excited states $|A1\rangle$ and $|B1\rangle$

close to each other or, more generally, to minimize their energy difference relative to the tunnel coupling, $|\Delta_0| \ll V_0$. Second, the interdot dynamics (tunneling) of the excited electron should prevail over the intradot dynamics (excitation) in order to form the stable transport DQD states via hybridization of the excited states of isolated QDs: $|g_{A(B)}| \ll V_0$. Two hybridized eigenstates are presented by even and odd superpositions of the states $|A1\rangle$ and $|B1\rangle$ with eigenenergies ε_- and ε_+ shifted down and up by V_0 , respectively, relative to the unperturbed energies $\varepsilon_{A1} \approx \varepsilon_{B1}$, as shown in Fig. 2(a). New transition frequencies are $\omega_{\pm} = \omega_{A(B)} \pm V_0$ (in the case of equal frequencies ω_A and ω_B). Third, by soft variation of the frequency detunings $\delta_A(t)$ and $\delta_B(t)$ between the DQD and the cavity, one should be able to set the appropriate regime of the optical driving. The resonant regime for which $|\delta_-| = |\omega_c - \omega_-| \ll |g_{A(B)}|$ or $|\delta_+| = |\omega_c - \omega_+| \ll |g_{A(B)}|$ assures fast population inversion of the qubit states through the optically induced electron transfer via one of the hybridized states. However, in that regime the electron demonstrates stroboscopic behavior being localized in the logical subspace at a discrete set of times only. On the other hand, the off-resonant regime for which $|\delta_{\pm}| \gg |g_{A(B)}|$ provides rather slow but nearly continuous evolution of the qubit state vector and, as a consequence, gives the possibility of its arbitrary in-plane rotation.

Numerical solutions of Eq. (3) for both regimes are presented in Fig. 4 for a given set of parameters: $c_k(0) = \delta_{k,A0}$, $g_A = g_B \equiv g = 6 \times 10^{-4} \omega_c$, $\delta_{Am} = 0.03 \omega_c$, $\delta_{Bm} = 0.015 \omega_c$, $V_0 = 0.008 \omega_c$, $V_m = 0$, and $\tau_0 = 50 \omega_c^{-1}$ ($\delta_{k,A0}$ is the Kronecker δ symbol). Choosing $\delta_{A0} = \delta_{B0} = V_0$, we tune the upper hybridized DQD state to the exact resonance with the cavity, $\omega_c = \omega_+$, and realize the three-level (or Λ) resonant scheme, as shown in Fig. 4(a). In this case, the voltage pulse duration required for the qubit inversion (or, equivalently, the operation time) is $\tau_p = 5.16 \times 10^3 \omega_c^{-1}$. Otherwise, if one sets $\delta_{A0} = \delta_{B0} = 0$, the cavity frequency falls just in the middle of the doublet of the hybridized state energies giving rise to the off-resonant electron transfer [see Fig. 4(b)] where now $\tau_p = 3.5 \times 10^4 \omega_c^{-1}$ that is by one order of magnitude longer than in the resonant case. As was expected, the time dependencies of the probabilities p_k resemble those obtained elsewhere for ramp pulses (cf., Ref. [27]). The transfer frequencies are given with good accuracy by the expressions $\Omega_{\text{res}} = |g|/\sqrt{2}$ and $\Omega_{\text{off-res}} = |g|^2/V_0$, while the pulse times are calculated according to the simple formulas $\tau_p = \pi\sqrt{2}/\Omega_{\text{res}}$ and $\tau_p = \pi/2\Omega_{\text{off-res}}$ for resonant and off-resonant cases, respectively. However, as long as the photon still populates the cavity after the transfer is completed, our qubit undergoes some unwanted perturbation at $t \geq \tau_p$. Its influence on the qubit dynamics is manifested in weak off-resonant oscillations of the populations p_{B0} and p_{B1} . The amplitude of those oscillations, as in the storage case, is defined by the detuning. Besides, it also depends on the tunneling V_0 that gives a possibility to optimize the transfer for some values of V_0 . In Fig. 5, we plot the minima and maxima of p_{B0} as functions of V_0 for the resonant scheme taken over the time interval $0 \leq t \leq 5 \times 10^4 \omega_c^{-1}$. As was mentioned above, the excited electron does not penetrate in the QD B for small tunnelings, $V_0 \leq |g_{A(B)}|$, and the population of the

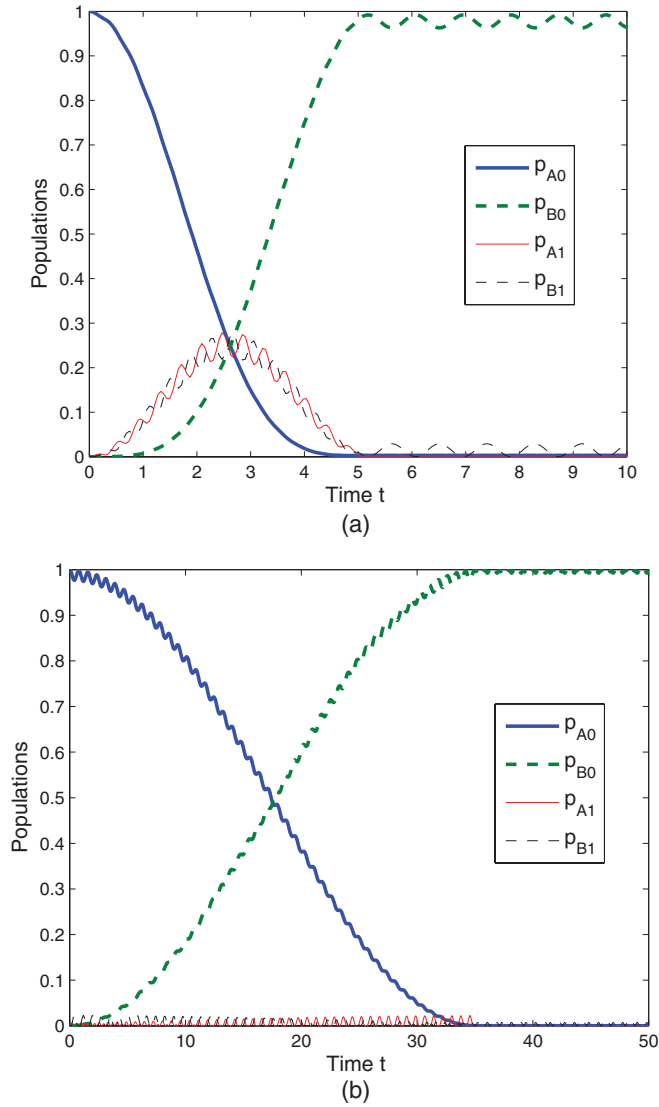


FIG. 4. (Color online) The NOT realizations in the DQD in (a) resonant and (b) off-resonant cases. The pulse and structure parameters are $g_{A(B)} = 6 \times 10^{-4} \omega_c$, $V_0 = 8 \times 10^{-3} \omega_c$, and $\tau_0 = 50 \omega_c^{-1}$. The time t is given in units of $10^3 \omega_c^{-1}$. The NOT pulse durations are $\tau_p = 5.16 \times 10^3 \omega_c^{-1}$ for (a) and $\tau_p = 3.5 \times 10^4 \omega_c^{-1}$ for (b).

state $|B0\rangle$ remains close to zero. At larger V_0 , both functions oscillate in phase slightly below unity. Obviously, choosing the tunneling value for which those functions simultaneously achieve their maxima, one may concentrate the population p_{B0} close to the unity. For example, for $V_0 = 6.7 \times 10^{-3} \omega_c$ one has $0.974 \leq p_{B0} \leq 0.994$ over the whole time domain. In the off-resonant scheme, as usual, the amplitude error is very small and additional optimization is not required.

The second gate we are going to simulate is the phase shift of one of the logical states relative to another one. As we have mentioned, the cavity photon produces slow phase evolution of the qubit in the off-resonant regime according to Eq. (7). To generate a relative phase shift and to accelerate phase dynamics one may apply the voltage pulses with nonequivalent detunings, $\delta_{A0} \neq \delta_{B0}$, which are smaller than δ_{Am} and δ_{Bm} but still large compared to the tunneling V_0 to suppress the

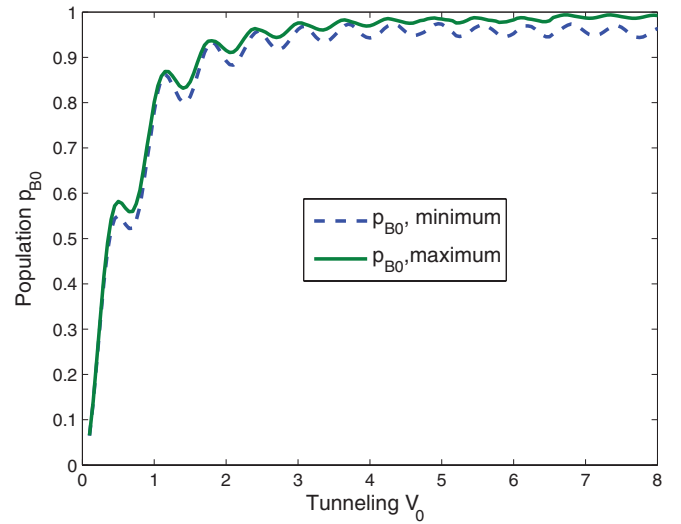


FIG. 5. (Color online) The dependencies of upper and lower bounds of the final state probability p_{B0} for the inversion $|A0\rangle \rightarrow |B0\rangle$ on the tunneling V_0 given in units of $10^{-3} \omega_c$. The pulse and structure parameters are the same as in the Fig. 4(a).

interdot electron transfer. Such off-resonant phase evolution brings about a continuous accumulation of the relative phase at moderate rates. Besides, the resonantly driven phase rotations are also possible. As an example of the fast phase dynamics we demonstrate the phase shift by π of the state $|B0\rangle$ relative to the state $|A0\rangle$. This operation can be performed via the resonant cyclic electron transition from the state $|B0\rangle$ to the state $|B1\rangle$ and back. Unlike for the inversion, there we apply strongly asymmetric driving [Fig. 2(b)] with negligible interdot tunneling, $|\Delta_0| \gg V_0$. As is known from the theory of two-level systems, the state $|B0\rangle$ gains in this case the relative phase multiplier $\exp(-i\pi)$. At the same time, the equivalent optical transition in the QD A should be suppressed. Numerical simulation of the phase dynamics for the initial DQD state $2^{-1/2}(|A0\rangle + |B0\rangle)$ with the system parameters $\delta_{Am} = \delta_{Bm} = 0.03 \omega_c$, $\delta_{A0} = 0.03 \omega_c$, $\delta_{B0} = 0$, $V_0 = 10^{-4} \omega_c$, and $\tau_p = 5.28 \times 10^3 \omega_c^{-1}$ (remaining values are taken as for the NOT operation) is shown in Fig. 6. At the end of the pulse, the relative phase of the state $|B0\rangle$ achieves a value of 3.1416 that means very accurate realization of the phase gate. With that, residual population redistribution caused by the finite tunneling amounts to the final probabilities $p_{A0} = 0.507$ and $p_{B0} = 0.493$ slightly different from their ideal values $p_{A0} = p_{B0} = 0.5$. Again, the amplitude correction can be performed by the tunneling suppression. Namely, the lowering of V_0 by one order of magnitude results in negligible amplitude error of about 10^{-4} only.

Apart from the two main regimes considered above, several important quantum operations can be efficiently realized under the intermediate regime with moderate detunings. We illustrate it by the Hadamard rotation (\hbar pulse or $\pi/4$ pulse) performed in two steps. At the first step, the initial state $|A0\rangle$ is transformed into the state $2^{-1/2}(|A0\rangle - i|B0\rangle)$ (the operating parameters are given in Fig. 7). At the second step, the fast relative phase shift $\delta\theta = \pi/2$ of the state $|B0\rangle$ compensating the multiplier $\exp(-i\pi/2)$ is achieved according to the scheme described above.

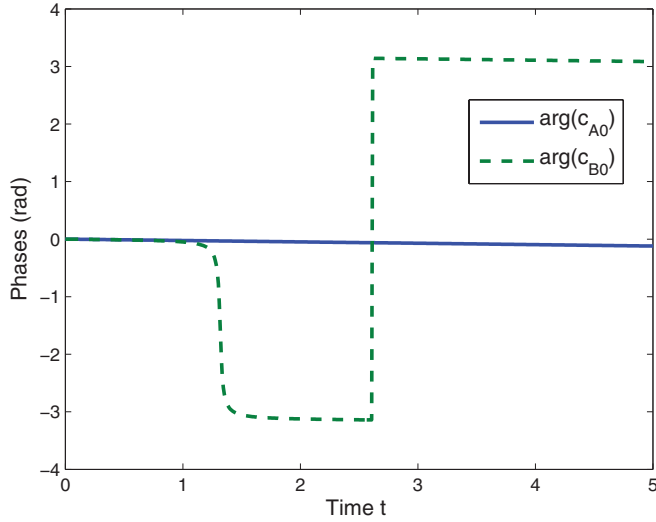


FIG. 6. (Color online) The resonant phase evolution of the qubit being in the equally-weighted superposition of logical states. The slow off-resonant phase shifts, Eq. (7), are seen as small identical linear drops in both curves. The time t is given in units of $10^3 \omega_c^{-1}$.

The considered gates (i.e., NOT, phase shift and Hadamard gates) form the so-called universal set, enabling one to approximate arbitrary single-qubit rotation. In order to implement arbitrary quantum operation, one is to add to the universal set a nontrivial two-qubit gate like the controlled NOT (CNOT) [2]. Let the control qubit be presented by the ground states $|A0\rangle$, $|B0\rangle$ of the first DQD while the ground states $|A0'\rangle$, $|B0'\rangle$ of the second DQD (whose parameters are supplied with prime) encode the target qubit. The DQDs are supposed to be placed at large distance from each other so that the

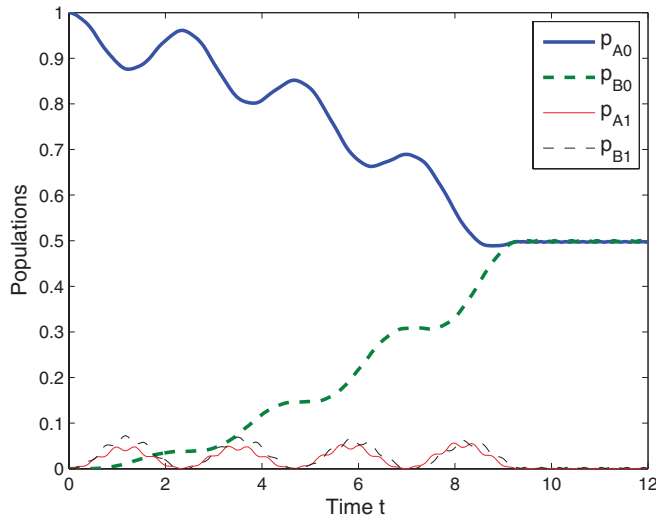


FIG. 7. (Color online) The first step of the Hadamard gate implementation amounting to the formation of the equally-weighted superposition of logical states. The pulse and structure parameters are $g_A = g_B = 6 \times 10^{-4} \omega_c$, $\delta_{A0} = \delta_{B0} = 5.6 \times 10^{-3} \omega_c$, $V_0 = 8 \times 10^{-3} \omega_c$, and $\tau_0 = 50 \omega_c^{-1}$. The pulse duration is $\tau_p = 9.36 \times 10^3 \omega_c^{-1}$. At the second step, the relative phase shift $\delta\theta = -\pi/2$ should be removed. The time t is given in units of $10^3 \omega_c^{-1}$.

direct electron-electron interaction is negligible. The two-qubit cavity system starts at $t = 0$ from its general state

$$|\Psi(0)\rangle = c_{A0,A0',1}|A0,A0',1\rangle + c_{A0,B0',1}|A0,B0',1\rangle + c_{B0,A0',1}|B0,A0',1\rangle + c_{B0,B0',1}|B0,B0',1\rangle. \quad (8)$$

The Hamiltonian governing the evolution of the two-qubit state is $H_{2q} = H_q + H'_q + H_c$. At first glance, there are no apparent terms responsible for the correlations between qubits since we neglect the Coulomb repulsion between DQD electrons. Nevertheless, the single-qubit Hamiltonians H_q and H'_q contain two common parameters (viz., the photon operators a and a^\dagger). The influence of these operators on the two-qubit dynamics becomes crucial in the single-photon case. Formally, the presence ($n = 1$) or the absence ($n = 0$) of the photon in the cavity mode means the driving field for qubits to be switched on or off, respectively, due to the multiplier \sqrt{n} in the expression for a . Therefore, if the first (control) qubit being in the defined logical state absorbs the photon from the cavity, transforming n from 1 to 0, the second (target) qubit cannot be driven. This observation can be applied to construct conditional two-qubit operations.

Using the principle outlined above, we have developed the following algorithm for the CNOT gate on a pair of the DQD qubits coupled to the same cavity mode. Initially, we convert the ground state $|A0\rangle$ of the first DQD (or the logical state $|0\rangle$ of the control qubit) to its auxiliary excited state $|A1\rangle$ to achieve the required photon absorption. The performance of this step is completed by the choice of the detuning dynamics that we call the a pulse (in fact, $\pi/2$ pulse). Namely, we drive the resonant transition $|A0\rangle \leftrightarrow |A1\rangle$ while keeping the transition $|B0\rangle \leftrightarrow |B1\rangle$ far from the resonance with the cavity as it was already done for the fast phase rotation. As a result, the electron staying in the state $|A0\rangle$ goes to the auxiliary state $|A1\rangle$ via full photon absorption by the control DQD

$$|A0,A0',1\rangle \xrightarrow{a} |A1,A0',0\rangle, \quad |A0,B0',1\rangle \xrightarrow{a} |A1,B0',0\rangle. \quad (9)$$

With that, if the electron occupies the state $|B0\rangle$ of the first DQD (or the logical state $|1\rangle$ of the control qubit), the a pulse does not excite it because the transition $|B0\rangle \leftrightarrow |B1\rangle$ is largely detuned from the cavity

$$|B0,A0',1\rangle \xrightarrow{a} |B0,A0',1\rangle, \quad |B0,B0',1\rangle \xrightarrow{a} |B0,B0',1\rangle. \quad (10)$$

Thus, at the end of the single a pulse we obtain an entangled state of the electron-photon system that includes two components (i.e., excited control DQD + empty cavity and nonexcited control DQD + one-photon cavity). Next, we make the target DQD close to the resonance with the cavity to realize the NOT gate, as it is described above. The state components (9) with $n = 0$ do not evolve since the empty cavity cannot drive the population inversion in the target DQD. In contrast, the state components (10) with $n = 1$ undergo the action of the π pulse that inverts the target qubit

$$|B0,A0',1\rangle \xrightarrow{\pi'} |B0,B0',1\rangle, \quad |B0,B0',1\rangle \xrightarrow{\pi'} |B0,A0',1\rangle. \quad (11)$$

Finally, we apply the second a pulse to disentangle the control qubit from the cavity by returning the photon from the control DQD back to the cavity mode. The result of the action of the above a - π' - a pulse sequence on the two-qubit basis is

summarized below:

$$\begin{aligned}
|A0, A0', 1\rangle &\xrightarrow{a} |A1, A0', 0\rangle \xrightarrow{\pi'} |A1, A0', 0\rangle \xrightarrow{a} |A0, A0', 1\rangle, \\
|A0, B0', 1\rangle &\xrightarrow{a} |A1, B0', 0\rangle \xrightarrow{\pi'} |A1, B0', 0\rangle \xrightarrow{a} |A0, B0', 1\rangle, \\
|B0, A0', 1\rangle &\xrightarrow{a} |B0, A0', 1\rangle \xrightarrow{\pi'} |B0, B0', 1\rangle \xrightarrow{a} |B0, B0', 1\rangle, \\
|B0, B0', 1\rangle &\xrightarrow{a} |B0, B0', 1\rangle \xrightarrow{\pi'} |B0, A0', 1\rangle \xrightarrow{a} |B0, A0', 1\rangle,
\end{aligned} \tag{12}$$

that is just the CNOT gate. In the expressions (9)–(12) we have omitted phase multipliers assuming that those will be compensated by appropriate timing and/or by auxiliary single-qubit phase shifts.

where

$$\begin{aligned}
G &= \begin{pmatrix} g_A e^{i\delta\varphi_A} & 0 & 0 & 0 \\ 0 & 0 & g_A e^{i\delta\varphi_A} & 0 \\ 0 & g_B e^{i\delta\varphi_B} & 0 & 0 \\ 0 & 0 & 0 & g_B e^{i\delta\varphi_B} \end{pmatrix}, & G' &= \begin{pmatrix} g'_A e^{i\delta\varphi'_A} & 0 & 0 & 0 \\ 0 & g'_B e^{i\delta\varphi'_B} & 0 & 0 \\ 0 & 0 & g'_A e^{i\delta\varphi'_A} & 0 \\ 0 & 0 & 0 & g'_B e^{i\delta\varphi'_B} \end{pmatrix}, \\
W &= - \begin{pmatrix} 0 & V e^{i\delta\Delta} & 0 & 0 \\ V e^{-i\delta\Delta} & 0 & 0 & 0 \\ 0 & 0 & 0 & V e^{i\delta\Delta} \\ 0 & 0 & V e^{-i\delta\Delta} & 0 \end{pmatrix}, & W' &= - \begin{pmatrix} 0 & V' e^{i\delta\Delta'} & 0 & 0 \\ V' e^{-i\delta\Delta'} & 0 & 0 & 0 \\ 0 & 0 & 0 & V' e^{i\delta\Delta'} \\ 0 & 0 & V' e^{-i\delta\Delta'} & 0 \end{pmatrix}
\end{aligned}$$

and O is the 4×4 zero matrix (the bar denotes Hermitian conjugation). The parameters of the matrix entries are defined in complete analogy with those in Eq. (3).

Taking into account the results of the single-qubit simulations we design the detuning and tunneling pulses for the CNOT gate as follows. The positions, envelopes, and durations of each pulse are defined by Eq. (4) where the transformation $t \rightarrow t - t_0$ ($t_0 \geq 0$ is the start time of a given pulse) has to be done. For the control DQD we set the parameters of the a pulse, $\delta_{Am} = 0.03\omega_c$, $\delta_{A0} = 0$, $\delta_{Bm} = \delta_{B0} = 0.03\omega_c$, $V_m = 10^{-5}\omega_c$, $V_0 = 10^{-4}\omega_c$, $\tau_p = 2.64 \times 10^3 \omega_c^{-1}$, and fix the delay time between the first and the second a pulses as $\tau_{\text{delay}} = 5.25 \times 10^3 \omega_c^{-1}$. The resonant π pulse on the target qubit is performed given $\delta'_{Am} = \delta'_{Bm} = 0.03\omega_c$, $\delta'_{A0} = \delta'_{B0} = V'_0$, $V'_m = 1.5 \times 10^{-5}\omega_c$, $V'_0 = 8 \times 10^{-3}\omega_c$, and $\tau_p = 5.16 \times 10^3 \omega_c^{-1}$. The delay time is taken slightly longer than the inversion time in order to avoid the overlapping of the pulses ($\tau_0 = 50\omega_c^{-1}$ for all types of pulses). The populations of four logical two-qubit states found numerically are plotted in Fig. 8 in the upper panel as functions of time. The middle and bottom panels in Fig. 8 reproduce the detuning and tunneling pulse profiles, respectively. As is clearly seen, the proposed scheme works with high accuracy ($p_{\text{CNOT}} \geq 0.99$). Besides, it is surprising that the phase accumulation is zero, and additional correction is not required. Thus, the total gate time is $\tau_{\text{CNOT}} \approx 1.044 \times 10^4 \omega_c^{-1}$ that is of the same order as for the intermediate single-qubit gates.

Note, that close strategy was developed for conditional two-qubit rotations of the atomic qubits traveling via the

We check the proposed scheme by numerical solution of the Schrödinger equation with the Hamiltonian H_{2q} in the basis of two four-level DQDs: $|A0, A0', 1\rangle$, $|A0, B0', 1\rangle$, $|B0, A0', 1\rangle$, $|B0, B0', 1\rangle$, $|A0, A1', 0\rangle$, $|A0, B1', 0\rangle$, $|B0, A1', 0\rangle$, $|B0, B1', 0\rangle$, $|A1, A0', 0\rangle$, $|B1, A0', 0\rangle$, $|A1, B0', 0\rangle$, and $|B1, B0', 0\rangle$, where we have omitted the states corresponding to double excitations since there is only one photon in the cavity. In this truncated basis, the Hamiltonian 12×12 matrix has the following form:

$$H_q = \begin{pmatrix} O & G' & G \\ \bar{G}' & W' & O \\ \bar{G} & O & W \end{pmatrix}, \tag{13}$$

Fabry-Perot cavity [31]. In that case, however, the photon exchange between the atom and the cavity directly results in the NOT operation. This was possible because the qubit logical states were ground and excited atomic states. Here, we need a more complex approach involving the auxiliary state since the logical states are both ground states of the DQD. Proposed conditionality can be classified as that based

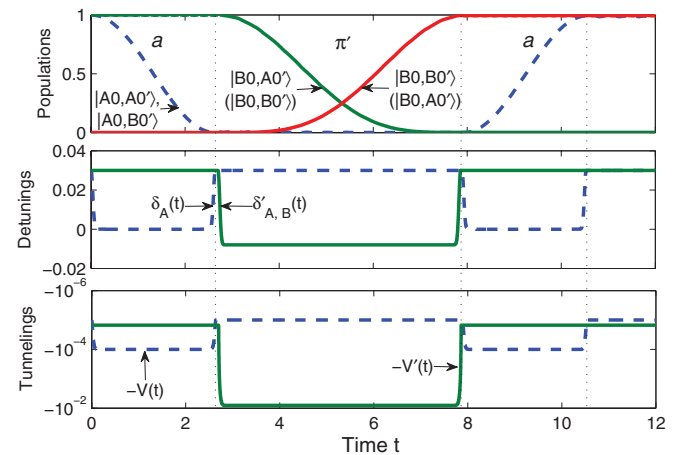


FIG. 8. (Color online) The time dependencies of logical state populations, detunings, and tunnelings in the CNOT gate realization. The detuning $\delta_B(t) \equiv 0.03\omega_c$ is not shown. The energy values in the plot are given in units of ω_c while the time t is given in units of $10^3 \omega_c^{-1}$.

on the control-qubit-state-dependent switching of the driving source for target qubit. In this case, the driver (cavity field) cannot be considered as an external substance independent from the qubits, as it was for the classical laser field containing many photons. Otherwise, the influence of the control qubit defines the photonic state of the cavity via strong quantum electrodynamic correlations between the matter and the field.

As an example of a quantum operation with larger qubit number we present the Shor's encoding realization involving nine DQD qubits [2]. Earlier, we exploited for that purpose a sequence of conditional probe electron transpositions caused by laser-induced excitations in an auxiliary QD structure [32]. Here, the probe electron is replaced by the cavity photon. As above, the logical qubit state $|0(1)\rangle$ is associated with the DQD state $|A(B)0\rangle$. At the beginning of the encoding procedure, the qubit (say, first) whose state we wish to protect is loaded in arbitrary superposition $|\Psi\rangle = c_0|0\rangle + c_1|1\rangle$ of its logical states. The remaining eight qubits are initialized in zero state. The encoding means the transformation of the state of a given qubit into highly entangled state $|\Psi\rangle_S = c_0|0\rangle_S + c_1|1\rangle_S$ spanned by the Shor code states (code words) $|0(1)\rangle_S = 2^{-3/2}(|000\rangle \pm |111\rangle)(|000\rangle \pm |111\rangle)(|000\rangle \pm |111\rangle)$ of a nine-qubit cluster. The pulse sequence performing this transformation includes three types of gates considered above (viz., h pulse, a pulse, and π pulse). We supply them by subscripts indicating the site index of the qubit to which that gate should be applied. The desired sequence of gates has the form

$$U_S = U_0 U_1 U_4 U_7, \quad (14)$$

where $U_0 = a_1 \pi_4 \pi_7 a_1$, $U_k = h_k a_k \pi_{k+1} \pi_{k+2} a_k$ ($k = 1, 4, 7$), and the operators act from the left to the right. The first operator U_0 realizes two subsequent CNOT gates with the first qubit as the control qubit and with the fourth and seventh qubits as the target qubits to entangle these head cluster qubits. Next, the operators U_k ($k = 1, 4, 7$) generate entanglement among k th, $k + 1$ th, and $k + 2$ th qubits via CNOT gates using the k th (head) qubit as the control qubit and the $k + 1$ th and $k + 2$ th qubits as the target qubits. Note that the application of Hadamard gates before CNOT gates in U_k establishes the required Shor's form of the code states; otherwise we would obtain the generalized nine-qubit GHZ (or Schrödinger cat) states.

Using the approach described, one may accomplish arbitrary quantum gate. For example, the three-qubit Toffoli gate (CCNOT) implementation requires the pulse sequence $U_{\text{CCNOT}} = a_1 a_2 \pi_3 a_2 a_1$ that inverts the third (target) qubit if and only if the first and the second (control) qubits are both loaded in the logical states one. The standard decomposition of the CCNOT into the sequence of universal gates includes ten single-qubit rotations and six CNOT operations [2]. Here, only five fast manipulations provide the realization of this important gate. This fact enables one to characterize our scheme as versatile and economic.

IV. DISCUSSION

In this section, we briefly discuss the feasibility of the proposed qubit taking into account the latest experimental breakthroughs in given areas of research. In recent years, noticeable progress was achieved in placement of the QDs in

the body of semiconductor microcavities and nanocavities. To optimize the qubit-cavity coupling, it is necessary to achieve high spatial matching of the QD and a cavity field antinode. Against routine Stranski-Krastanow strain-induced stochastic condensation of disordered QD assemblies in InGaAs/GaAs heterostructures [1,11,12], the advanced methods of site-controlled QD nucleation [14–18] bring about the formation of regular arrays of the QDs. In those methods, the position of the QD (and partially its geometry) is determined (e.g., by adatom surface diffusion [14] or via selective surface patterning by lithographic means [15–17]). An alternative framework uses the optical identification of a single QD in the substrate followed by cavity formation around the QD [18]. The characteristic size of obtained QDs is varied from several to several tens of nanometers. Corresponding electron intrasubband transition frequencies lie in the range from several hundreds to several tens of meV. Note, that the conduction band mismatch for InGaAs/GaAs heterostructures (and, consequently, the QD potential depth) is about 250 meV. The cavity mode region is usually confined to several hundreds of nanometers in photonic crystal defects. This enables one to consider the quantized field strength (and, consequently, the coupling value) as uniform over the QD volume given the QD is accurately placed in the field antinode. Further, the QDs in the second InGaAs layer of heterostructure are formed strictly above the QDs in the first InGaAs layer [16]. Moreover, the upper QD will closely reproduce the form and the size of the bottom one. Thus, combining all those techniques, one can synthesize the highly symmetric DQD structure studied in this work as a vertical stack of two nearly identical single QDs, as shown in Fig. 1. The single-electron injection in the DQD [30] together with fine manipulation of its frequency (and tunneling) can be realized by the electrostatic gate(s) [19,20]. As was demonstrated in the work [19], the parameters of QDs in different layers are tuned independently thus making the control over qubit dynamics more flexible.

Let us estimate the working parameters of our qubit. The DQD transition frequency $\omega_{A(B)m}$ can be evaluated from the difference $\Delta\varepsilon_{10} = 3\pi^2 \hbar^2 / 2m^* a^2 \approx (m_e/m^*)a^{-2}$ (in eV) between the ground and first excited state energies of the single cubic QD, where m_e is the free electron mass, m^* is the effective electron mass, and the cubic side length a is taken in nanometers. It defines the resonator frequency as $\omega_c \approx \omega_{A(B)m} \approx \Delta\varepsilon_{10}/\hbar$. For $a = 15$ nm (the mean value of a in experiments) and $m^* \approx 0.067m_e$ in $\text{In}_x\text{Ga}_{1-x}\text{As}$ ($x < 0.5$) we obtain $\hbar\omega_c \approx 80$ meV. On other hand, the Rabi frequency is $g \sim eaE_{c,0}$, where the antinode field strength $E_{c,0}$ is defined by the cavity material and geometry. Using $E_{c,0} = 10$ V/cm, one has the following estimation for the coupling coefficient, $g \approx 1.5 \times 10^{-5}$ eV. In our simulations, we have used $g = 6 \times 10^{-4}\omega_c$ or 4.8×10^{-5} eV for obtained ω_c that agrees well with the value just found. Further, the switch-on tunneling used in the paper is $V_0 = 0.008\omega_c \approx 0.64$ meV and also corresponds to the values measured in experiments. Since V_0 depends on both the width l and the height ΔU of the potential barrier separating QD A and QD B this particular tunneling choice describes a lot of possible structure realizations. The $\delta_{A(B)m}$ and $\delta'_{A(B)m}$ of electrostatic detuning pulses are equal to $0.03\omega_c$ or 2.4 meV thus requiring application of gate voltages of several volts [20]. Finally, the fast single-qubit rotations

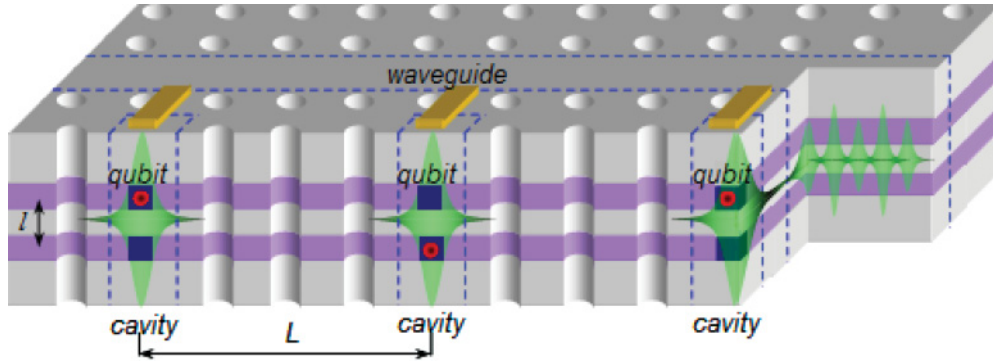


FIG. 9. (Color online) The schematics of the quantum register based on the array of DQD charge qubits. Each qubit is placed inside individual cavity. The interdot distance in DQD is l and the distance between neighboring qubits is L . All cavities are coupled to the waveguide formed in parallel to the qubit array. Both cavities and waveguide are photonic crystal defects which boundaries are marked by dashed lines. The overlapping between cavity and waveguide modes that results in the formation of the auxiliary hybridized mode is also shown.

(inversion and phase shift) are performed during the pulse time $\tau_p \approx 40$ ps while the two-qubit CNOT gate consumes the time $\tau_p \approx 100$ ps.

The scaling of our qubit can be achieved through manufacturing of ordered DQD arrays where each qubit is coupled to the cavity antinode and integrated with the voltage gates for its individual control. In Fig. 9 we present schematically one possible scalable design of the quantum register composed of our DQD charge qubits. The base of the register (i.e., some number of equally spaced DQDs) can be grown in InGaAs/GaAs heterostructure according to the technique described in Ref. [16]. Next, the photonic crystal lattice is lithographically patterned on the base by hole milling with cavities (missing hole defects) around each of DQDs and with waveguide (long line defect) near cavity array. We suppose that the cavity-waveguide coupling is much larger than the DQD-cavity coupling. Therefore, a stationary bus mode is formed via photon hopping between isolated cavity modes and waveguide mode [33]. We identify this hybridized mode with the resonator mode introduced in Secs. II and III.

There exist several decoherence sources that degrade the robustness of quantum gates in semiconductor DQD charge qubits. In our case, the most important among them are (i) phonon-induced qubit relaxation and dephasing, (ii) gate-induced qubit dephasing, (iii) dephasing caused by uncontrollable interaction between qubits, (iv) evolution errors produced by pulse imperfections, and (v) photon relaxation from the cavity (perhaps enforced by gates and other circuitry). Below we give estimations on the decoherence times for each of them.

(i) According to the Ref. [34] the phonon relaxation time $\tau_{1,\text{ph}} \sim \gamma^{-1}$ in self-assembled QDs varies from 10^{-9} s to 10^{-8} s and depends strongly on structure parameters. Phonon dephasing is usually characterized by the time $\tau_{2,\text{ph}} \sim 10^{-9}$ s at liquid helium temperature. The number of quantum operations is defined through the ratio $\min\{\tau_{1,\text{ph}}, \tau_{2,\text{ph}}\}/\tau_p$. One sees that for $\tau_p \leq 10^{-10}$ s only several gates can be performed with high fidelity. However, mentioned decoherence times were found for bulk semiconductors. One may expect that in lithographically patterned thin slabs the phonon spectrum will be modified. To date, the experiments enable us to say that phonons do not prohibit observations of excitonic Rabi

oscillations in QDs [9], so at least amplitude coherence is conserved at moderate level.

(ii) The influence of metallic gate electrodes on charge dynamics in DQD was studied theoretically in Refs. [35] and [36] under different assumptions. Authors conclude that the electrostatic interaction between gate(s) and qubit results in rather slow dephasing of the latter. Provided that the distance between the gate and the qubit is large (≥ 100 nm) and the interdot barrier width is small (≤ 50 nm) the dephasing time τ_g ranges from 10^{-8} s to 10^{-7} s. This time is too long when compared with phonon-dephasing time $\tau_{2,\text{ph}}$ so one may safely neglect gate influence on the qubit at the given stage of research. For future applications the detrimental effects of the register circuitry including strong surface scattering in metallic gates should be studied in detail.

(iii) To suppress unwanted Coulomb correlations among the DQD electrons, the neighboring qubits should be located at the distance $L \gg l$ from each other. For example, the interdot distance l in [16] was approximately 10 nm and, therefore, L should be of the order of several microns. At large distance L , two DQD qubits interact mainly as two point charges. Coulomb repulsion energy of two electrons in neighbor DQD qubits (i th and $i+1$ th) is written $U_{k,l}^{e-e} = e^2/\kappa|\mathbf{r}_{i,k} - \mathbf{r}_{i+1,l}|$, where $\mathbf{r}_{i,k}$ is the radius vector of electron in i th DQD, κ is the dielectric constant, and $k,l = A,B$ are single-QD indices. The small difference $\Delta U^{e-e} = U_{AA}^{e-e} - U_{AB}^{e-e}$ between interaction energies corresponding to different two-electron configurations results in dephasing process [37]. Given $L \gg l$ it is easy to see that $\Delta U^{e-e}/U_{AA}^{e-e} \approx l^2/2L^2$. For example, if $L = 3 \mu\text{m}$ and $l = 30$ nm, we obtain for GaAs $U_{AA}^{e-e} = 2 \times 10^{-5}$ eV and $\Delta U^{e-e} = 10^{-9}$ eV. It corresponds to dephasing time $\tau_{e-e} \sim \hbar/\Delta U^{e-e}$ of hundreds of nanoseconds that is by three orders of magnitude slower than our operation times $\tau_p \leq 10^{-10}$ s.

(iv) Previously (see, e.g., Refs. [24] and [27]) we derived the analytical expression for the electron transfer probability in DQD as a function of pulse imperfections. In particular, resonant transfer error scales with frequency detuning δ as δ^2/g^2 while phase error behaves as δ/g . Despite the preserved coherence of the qubit in the presence of the detuning and timing uncertainties, we suppose these types of

errors to be quite serious especially for the resonant driving. Successful implementation of proposed operations requires fine electrostatic tuning of QD frequency with accuracy of 10^{-7} eV. The voltage pulse duration should be controlled with accuracy higher than 10^{-12} s.

(v) To date, the highest quality of $Q = 25\,000$ has been reported for the QD-doped nanobeam cavity against calculated quality $Q > 10^7$ for the undoped cavity [13]. Besides, the authors of Ref. [13] achieved the highest value of 2.1 of the ratio of the coupling coefficient g to the photon decay rate Γ_c and observed the vacuum Rabi splitting. At the same time, this value is too small for quantum computer applications. Here, we use the quality factor of $Q = 10^6$ that is by almost two orders of magnitude larger than that has been achieved in Ref. [13]. Currently, it remains an optimistic value for experimental realization. With that, we may say that it is a very expectable value in the near future in view of rapid technological progress in manufacturing of high-quality semiconductor resonators. A possible solution to quality improvement should consist in both material purification and geometry optimization of given system. We should also mention that introduced gates will diminish the quality factor so their design has to be carefully elaborated as well. For frequencies used in the paper ($\omega_c \approx 80$ meV) we obtain the photon relaxation time $\tau_c = \Gamma_c^{-1} = Q/\omega_c \sim 10^{-8}$ s. Keeping in mind that estimated operation times τ_p for quantum gates lie in the range of 10^{-11} – 10^{-10} s, several tens of quantum operations could be performed with the help of given localized photon before it will dissipate from the cavity. This is enough for proof-of-principle demonstrations. An alternative approach is to use single photon per single gate. In this case, the fidelity of the quantum operation will be much higher but the scheme will become more complex because of the need of controlled photon channelling in and out of the cavity before and after each operation. Here, we restrict our consideration by the first case as the simplest one. However, the formalism developed in Secs. II and III is valid for both cases.

The next serious challenge may arise in the selective population of resonant mode if one uses a structured waveguide composed of large number of elementary cavities [38]. This waveguide looks more suitable for interqubit coupling in comparison with nonmodified line-defect waveguides [33]. With that, the number of hybridized waveguide modes will increase with the number of cavities while the defect bandwidth depending only on the intercavity photon hopping strength will remain unchanged. As a result, the density of waveguide modes grows and the selective addressability of the photon mode used in our scheme becomes quite low. The authors of Ref. [38] demonstrated satisfactory resolution over waveguides composed of up to several hundreds of cavities. To overcome this general problem of hopping particles in a linear chain of identical sites one may destroy the identity to split the auxiliary mode from other ones [39].

Very recently, the experimental realization of two QD-doped cavities formed in the heterostructure-based photonic crystal and coupled by the waveguide has been reported by Thon *et al.* [40]. The QD excitonic spectra were independently tuned by electrostatic gates. The distance between cavities

(i.e., between working QDs) was about $3\ \mu\text{m}$. The given result substantiates the viability of our design. Being combined with the QD placement control [16], this technique can be directly used in the manufacturing of the large-scale quantum register proposed in this paper. Even now the experiment of Ref. [40] confirms many assumptions made in our model. Several of them still remain optimistic, namely those concerned with cavity properties and voltage pulse robustness.

As a final remark, we adopt the general secondary-quantized framework for qubits in the cavity instead of the description of driven DQDs under some microscopic model in the coordinate-time space. Such an approach is becoming more and more popular transforming into a routine and commonly applied tool for the qubit analysis. All of the relevant parameters in Eq. (1) are extracted from experimental testing of concrete structure. Thus, the couplings $g_{A,B}$ can be identified with the vacuum Rabi splitting in photon transmission experiments; the QD frequencies $\omega_{A,B}$ and interdot tunnelings $V_{0,m}$ are found in luminescence observation; the values of the dissipation coefficients γ and Γ_c follow from emission studies. The voltage-induced detuning and tunneling dynamics can be tabulated in similar fashion.

Here, we don't examine the detrimental effects on the quantum operations such as those caused by the electron continuum and the DQD asymmetry. Also, we obtain our results under coherent approximation neglecting the dissipative channels in the photon dynamics. Moreover, we restrict ourselves by the simple case when only one qubit interacts with the cavity. The situation where two or more qubits are simultaneously brought in resonance with the cavity looks much more complex and interesting and may allow alternative realizations of multiqubit gates. All of those questions are topics for future treatments.

V. CONCLUSION

In this paper, we have considered a mechanism of the charge qubit state control using the quantum field in the semiconductor cavity. Apart from accurate QD positioning inside the cavity, it is based on the ability to engineer the voltage pulse sequences needed for robust electrostatic tuning of the qubit frequency in resonance with the cavity. Modern techniques have already approached the level at which the given scheme may be realized. It would drastically simplify the electron-state rotation in comparison with other schemes of optically controlled charge qubits because it does not require the laser's application.

At this moment, the strong-coupling regime for single-electron charge qubits has not yet been demonstrated. However, the observation of the successful development of existing QD exciton qubits in cavities allows us to consider the perspective of building up of their charge analog as an achievable, interesting, and attractive aim. We hope that our proposal encourages experimenters to explore this problem further.

ACKNOWLEDGMENTS

The author wishes to thank Professor A. A. Orlikovsky and I. Y. Kateev for interesting and stimulating discussions.

- [1] B. A. Joyce, P. C. Kelires, A. G. Naumovets, and D. D. Vvedensky, *Quantum Dots: Fundamentals, Applications, and Frontiers* (Springer, Dordrecht, 2003).
- [2] M. A. Nielsen and I. L. Chuang, *Quantum Computation and Quantum Information*. (Cambridge University Press, Cambridge, 2000).
- [3] S. Laurent *et al.*, *Appl. Phys. Lett.* **87**, 163107 (2005).
- [4] A. Barenco, D. Deutsch, A. Ekert, and R. Jozsa, *Phys. Rev. Lett.* **74**, 4083 (1995).
- [5] L. Fedichkin, M. Yanchenko, and K. A. Valiev, *Nanotechnology* **11**, 387 (2000).
- [6] J. M. Taylor *et al.*, *Nature Phys.* **1**, 177 (2005).
- [7] W. G. van der Wiel *et al.*, *New J. Phys.* **8**, 28 (2006).
- [8] H. J. Krenner *et al.*, *New J. Phys.* **7**, 184 (2005).
- [9] S. M. de Vasconcellos *et al.*, *Nature Photon.* **4**, 545 (2010).
- [10] S. Noda, M. Fujita, and T. Asano, *Nature Photon.* **1**, 449 (2007).
- [11] T. Yoshie *et al.*, *Nature (London)* **432**, 200 (2004).
- [12] W. C. Stumpf *et al.*, *Appl. Phys. Lett.* **90**, 231101 (2007).
- [13] R. Ohta *et al.*, *Appl. Phys. Lett.* **98**, 173104 (2011).
- [14] Z. G. Xie and G. S. Solomon, *Appl. Phys. Lett.* **87**, 093106 (2005).
- [15] P. Gallo *et al.*, *Appl. Phys. Lett.* **92**, 263101 (2008).
- [16] C. Schneider *et al.*, *Appl. Phys. Lett.* **94**, 111111 (2009).
- [17] N. L. Dias *et al.*, *Appl. Phys. Lett.* **98**, 141112 (2011).
- [18] S. M. Thon *et al.*, *Appl. Phys. Lett.* **94**, 111115 (2009).
- [19] H. Kim, S. M. Thon, P. M. Petroff, and D. Bouwmeester, *Appl. Phys. Lett.* **95**, 243107 (2009).
- [20] A. Faraon, A. Majumdar, H. Kim, P. Petroff, and J. Vuckovic, *Phys. Rev. Lett.* **104**, 047402 (2010).
- [21] D. Englund, D. Fattal, E. Waks, G. Solomon, B. Zhang, T. Nakaoka, Y. Arakawa, Y. Yamamoto, and J. Vuckovic, *Phys. Rev. Lett.* **95**, 013904 (2005).
- [22] L. A. Openov, *Phys. Rev. B* **60**, 8798 (1999).
- [23] J. H. Oh, D. Ahn, and S. W. Hwang, *Phys. Rev. A* **62**, 052306 (2000).
- [24] A. V. Tsukanov and L. A. Openov, *Fiz. Tekh. Poluprovodn. (St. Petersburg)* **38**, 94 (2004); *Semiconductors* **38**, 91 (2004).
- [25] E. Paspalakis, Z. Kis, E. Voutsinas, and A. F. Terzis, *Phys. Rev. B* **69**, 155316 (2004).
- [26] A. M. Basharov and S. A. Dubovis, *Opt. Spektrosk.* **99**, 802 (2005); *Opt. Spectrosc. (Russia)* **99**, 770 (2005).
- [27] A. V. Tsukanov, *Phys. Rev. B* **73**, 085308 (2006).
- [28] M. S. Sherwin, A. Imamoglu, and T. Montroy, *Phys. Rev. A* **60**, 3508 (1999).
- [29] X.-Y. Lu, J. Wu, L.-L. Zheng, and Z.-M. Zhan, *Phys. Rev. A* **83**, 042302 (2011).
- [30] E. T. Croke *et al.*, *Appl. Phys. Lett.* **96**, 042101 (2010).
- [31] J. M. Raimond, M. Brune, and S. Haroche, *Rev. Mod. Phys.* **73**, 565 (2001).
- [32] A. V. Tsukanov, *J. Phys. Condens. Matter* **21**, 055501 (2009).
- [33] A. Faraon *et al.*, *Appl. Phys. Lett.* **90**, 073102 (2007); *New J. Phys.* **13**, 055025 (2011).
- [34] E. A. Zibik *et al.*, *Nature Mater.* **8**, 803 (2009).
- [35] S. R. Woodford, A. Bringer, and K. M. Indlekofer, *Phys. Rev. B* **76**, 064306 (2007).
- [36] S. Filippov, V. Vyurkov, and L. Fedichkin, *Physica E* **44**, 501 (2011).
- [37] V. Vyurkov, S. Filippov, and L. Gorelik, *Phys. Lett. A* **374**, 3285 (2010).
- [38] M. Notomi, E. Kuramochi, and T. Tanabe, *Nature Photon.* **2**, 741 (2008).
- [39] L. A. Openov and A. V. Tsukanov, *Fiz. Tekh. Poluprovodn. (St. Petersburg)* **39**, 235 (2005); *Semiconductors* **39**, 251 (2005).
- [40] S. M. Thon *et al.*, *Appl. Phys. Lett.* **99**, 161102 (2011).